GEOPHYSICS, VOL. 70, NO. 4 (JULY-AUGUST 2005); P. T57–T62, 8 FIGS.
10.1190/1.1988187

Two-dimensional finite-difference seismic modeling of an open fluid-filled fracture: Comparison of thin-layer and linear-slip models

Chunling Wu[1], Jerry M. Harris[1], Kurt T. Nihei[2], and Seiji Nakagawa[2]

ABSTRACT

Within the context of seismic wave propagation, fractures can be described as thin layers or linear-slip interfaces. In this paper, numerical simulations of elastic wave propagation in a medium with a single fracture represented by these two models are performed by 2D finite-difference codes: a variable-grid isotropic code for the thin-layer model and a regular-grid anisotropic code for the linear-slip model. Numerical results show excellent agreement between the two models for wavefields away from the fracture; the only discrepancy between the two is the presence of a slow wave traveling primarily within the fracture fluid of the thin-layer model. The comparison of the computational cost shows that modeling of the linear-slip model is more efficient than that of the thin-layer model. This study demonstrates that the linear-slip model is an efficient and accurate modeling approach for the remote seismic characterization of fractures.

INTRODUCTION

The presence of fractures critically affects the permeability of rocks and, therefore, the character of fluid flow in hydrocarbon reservoirs. Thus, fracture detection and characterization is very important in hydrocarbon recovery. Seismic modeling of fractured media is an efficient tool for investigating the possibilities of using seismic waves to characterize the fractures.

For purposes of seismic wave propagation, fractures are often described as linear-slip interfaces with displacement discontinuities (Schoenberg, 1980; Pyrak-Nolte, 1988). In the linear-slip model (LSM), it is assumed that a fracture can be represented by an interface across which the displacements caused by a seismic wave are discontinuous while the tractions remain continuous. The linear relationship between the jump in the displacement vector and the traction vector is determined by the fracture compliance tensor. Coates and Schoenberg (1995) introduced an equivalent medium theory approach for embedding a linear-slip interface within an anisotropic finite-difference (FD) code.

Alternatively, an open fluid-filled fracture can be represented by a thin fluid layer following the approach of Groenenboom and Fokkema (1998). For the thin-layer model (TLM), variable-grid FD methods (Moczo, 1989; Jastram and Behle 1991; Falk et al., 1996; Pitarka, 1999) can be used to smoothly vary the cell spacing from the far-field mesh to the vicinity of the fracture, thus approximating the fracture directly by a number of grid points (Groenenboom and Falk, 2000). This variable-grid approach for explicit modeling of open fluid-filled fractures requires more cells than the Coates-Schoenberg approach. However, the use of the variable grid around the fracture significantly reduces the number of extra cells needed to model the fracture, compared to a regular, very fine grid.

The purpose of this paper is to compare a variable-grid FD method for the TLM with the Coates-Schoenberg approach for the LSM to determine to what extent the TLM agrees with the LSM. Numerical results show that the agreement between the two models is excellent except for the existence of a slow fracture wave in the TLM. Two calculations also demonstrate that modeling the LSM is more efficient than modeling the TLM. The sections that follow present the methods and their comparison in greater detail.

METHODOLOGY

Variable-grid FD method for the TLM

FD seismic modeling is commonly based on regular grids. Grid spacing, and hence the computational effort, is determined by the smallest length scale to be modeled, usually

Presented at the 72nd Annual International Meeting, Society of Exploration Geophysicists. Manuscript received by the Editor January 2, 2003; revised manuscript received September 29, 2004; published online July 7, 2005.
[1]Stanford University, Department of Geophysics, 397 Panama Mall, Stanford, California 94305-2215. E-mail: clwu@pangea.stanford.edu; harris@pangea.stanford.edu.
[2]Lawrence Berkeley National Laboratory, Earth Sciences Division, 1 Cyclotron Road, MS 90-1116, Berkeley, California 94720. E-mail: ktnihei@lbl.gov; snakagawa@lbl.gov.

the shortest seismic wavelength. Explicitly modeling a fracture described by the TLM introduces a length scale (the fracture width), which is often two or three orders of magnitude smaller than the shortest seismic wavelength, thus greatly increasing the computational load and restricting calculations to models of very small overall dimensions. To overcome this problem, we apply a variable-grid FD scheme (Pitarka, 1999) for solving the 2D velocity-stress elastic-wave equation:

$$\begin{aligned}
\rho\frac{\partial v_x}{\partial t} &= \frac{\partial \tau_{xx}}{\partial x} + \frac{\partial \tau_{xz}}{\partial z},\\
\rho\frac{\partial v_z}{\partial t} &= \frac{\partial \tau_{xz}}{\partial x} + \frac{\partial \tau_{zz}}{\partial z},\\
\frac{\partial \tau_{xx}}{\partial t} &= (\lambda+2\mu)\frac{\partial v_x}{\partial x} + \lambda\frac{\partial v_z}{\partial z},\\
\frac{\partial \tau_{zz}}{\partial t} &= (\lambda+2\mu)\frac{\partial v_z}{\partial z} + \lambda\frac{\partial v_x}{\partial x},\\
\frac{\partial \tau_{xz}}{\partial t} &= \mu\left(\frac{\partial v_x}{\partial z} + \frac{\partial v_z}{\partial x}\right),
\end{aligned} \tag{1}$$

where v_x and v_z are the particle velocity components; τ_{xx}, τ_{xz}, and τ_{zz} are stress components; ρ is density; and λ and μ are the Lamé coefficients.

We use a simple FD gridding scheme to represent the x-z fracture plane. The plane is partitioned into (1) domains of fine grid spacing for resolving fractures, (2) domains of coarse grid spacing constrained by the shortest wavelength, and (3) transition regions where the grid spacing smoothly varies between these extremes (see Figure 1). The smooth refinement from the coarse grid to fine grid avoids the spurious reflection problems associated with sudden changes in grid spacing.

Solving the elastic wave equation on a variable grid requires the spatial derivatives in equation 1 to be approximated using a stretched stencil. Several techniques exist for efficiently calculating the coefficients for the stretched difference operators. We use the method proposed by Pitarka in 1999 (Appendix A)

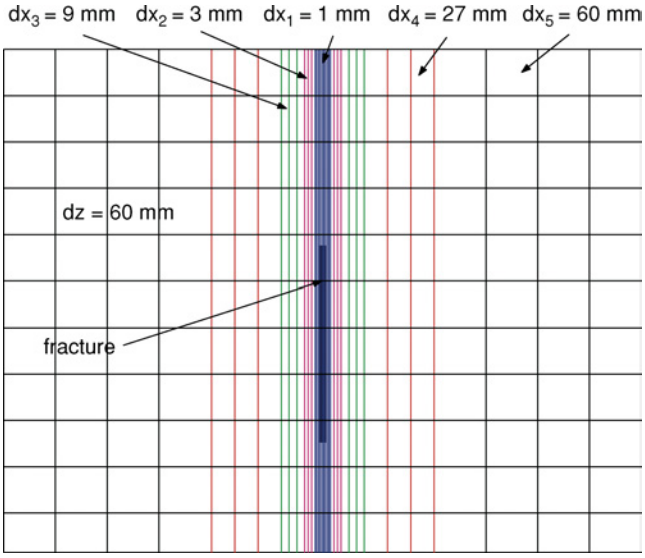

Figure 1. Grid spacing in the vicinity of a fracture. The horizontal grid spacing smoothly increases from 1 mm to 6 cm with a factor of 3 over a transition region 11.7 cm wide. The vertical grid spacing is 6 cm throughout the grid. The fracture dimensions are 4 mm width × 10.56 m length.

to precompute explicit fourth-order operators for all spatial locations. Since the mesh is only distorted along the x- and z-axes, coefficients are invariant along grid lines, reducing the memory required for stencil storage. The variable mesh is also staggered to increase stability and minimize numerical dispersion. The staggered scheme is crucial for handling solid-liquid contacts present in fractured media. Time derivatives are staggered across the velocity and stress variables and are approximated using an explicit second-order central difference operator.

To minimize numerical dispersion during the computation, the spatial discretization is chosen to satisfy the following inequality (Pitarka, 1999):

$$h_{max} < \frac{V_{min}}{5 f_{max}}, \tag{2}$$

where h_{max} is the maximum grid spacing, V_{min} is the lowest velocity in the media, and f_{max} is the maximum frequency of the propagating signal.

The stability condition for the 2D fourth-order staggered-grid FD scheme with constant grid spacing h is (Levander, 1988)

$$\Delta t < \frac{1}{\sqrt{2}(|\alpha_1| + |\alpha_2|)}\frac{h}{V_{max}} \tag{3}$$

or

$$\Delta t < 0.606\frac{h}{V_{max}},$$

where $\alpha_1 = 9/8$ and $\alpha_2 = -1/24$ are the inner and outer coefficients of the fourth-order approximation to the first derivative. V_{max} is the highest velocity in the media.

Through a series of numerical tests, we found that the variable-grid FD scheme used in this paper is stable when the temporal increment Δt is chosen to satisfy equation 3 with the minimum grid spacing in the variable grid.

Coates-Schoenberg approach for the LSM

To incorporate a fracture described by the LSM into an FD code, Coates and Schoenberg (1995) introduced an equivalent medium approach. In this approach, all FD grid cells containing a fracture are replaced by grid cells with equivalent anisotropic properties that model the fracture and host compliances (Figure 2).

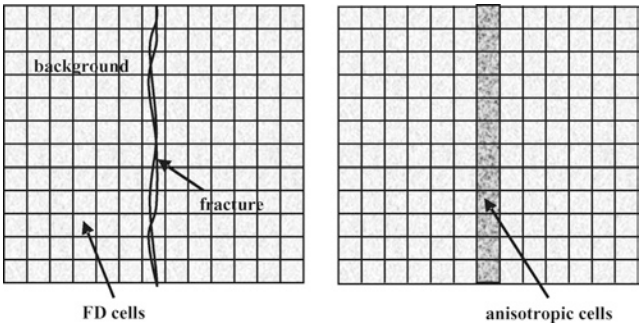

Figure 2. Representation of a vertical fracture in an FD model as a single column of anisotropic cells. The elastic constants for these cells are computed using the Coates-Schoenberg approach described in the text.

The variables required for the equivalent medium calculation in each FD cell are Lamé constants λ and μ of the background medium, the length of the fracture L (in two dimensions) in each cell, its orientation, and the normal and shear fracture compliances Z_N and Z_T, respectively.

For a vertical fracture with its normal in the x-direction, the four independent anisotropic elastic constants for a 2D model in the x-z plane are (Nihei, et al., 2001)

$$C_{ij}^{cell} = \begin{bmatrix} (\lambda+2\mu)(1-\delta_N) & \lambda(1-\delta_N) & 0 \\ \lambda(1-\delta_N) & (\lambda+2\mu)(1-r^2\delta_N) & 0 \\ 0 & 0 & \mu(1-\delta_T) \end{bmatrix}, \quad (4)$$

where $r = \nu/(1-\nu)$, $\delta_N = Z_N(\lambda+2\mu)/[L+Z_N(\lambda+2\mu)]$, $\delta_T = Z_T\mu/(L+Z_T\mu)$, and ν is the background Poisson's ratio. The equivalent medium described by equation 4 is transversely isotropic with a horizontal axis of symmetry (HTI media). A fracture oriented at an angle to the FD grid can also be modeled by applying a rotation transformation to equation 4, as described by Coates and Schoenberg (1995); this leads into a full anisotropic medium with six independent elastic constants in two dimensions.

After the equivalent medium properties of each cell are obtained, the standard FD scheme for anisotropic media can be applied. The code we used is a regular staggered-grid FD scheme with fourth-order spatial differencing and second-order temporal differencing.

OPEN FLUID-FILLED FRACTURE MODEL

Both the variable-grid FD method and the Coates-Schoenberg approach are used to model wave propagation in a medium with an open water-filled fracture to examine to what extent the TLM agrees with the LSM.

Figure 3 shows the model. A vertical water-filled fracture with 4 mm thickness and 10.56 m length is embedded in a homogeneous elastic medium. A monopole source (S), located at (12.78 m, 12 m), radiates a Ricker pulse with a central frequency of 3 kHz. Two receivers (R_1 and R_2) are located at (10.2 m, 18 m) and (6 m, 18 m). For variable-grid FD modeling of the TLM, the horizontal grid spacing smoothly increases from 1 mm to 6 cm with a factor of 3 over a transition region 11.7 cm wide in the vicinity of the fracture; the vertical grid spacing is 6 cm throughout the grid (Figure 1). For the Coates-Schoenberg approach of the LSM, a constant FD grid spacing of 6 cm is used in both the x- and z-directions. The calculation of effective medium properties of the LSM cells containing the fracture is based on the transverse fracture compliance $Z_T = \infty$, and the normal fracture compliance $Z_N = h/K = 0.004$ m/2.25 GPa (h is the fracture width and K is the bulk modulus of the fluid). The parameters of the background medium are $\lambda = 7.6194$ GPa, $\mu = 18.152$ GPa, and $\nu = 0.148$ calculated from the P-wave velocity V_p, S-wave velocity V_s, and density ρ.

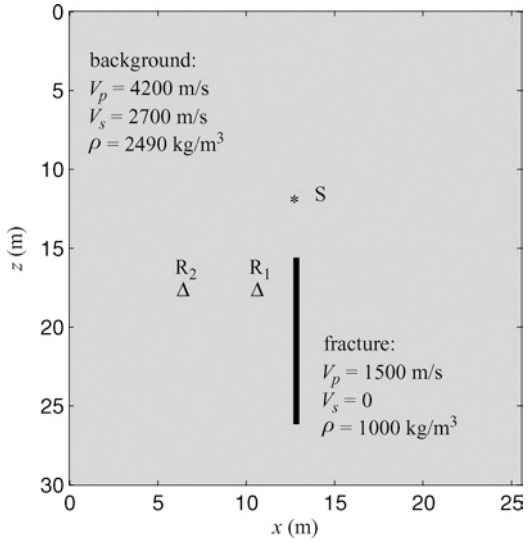

Figure 3. A vertical fracture model.

Snapshots of horizontal and vertical particle-velocity components of the TLM and the LSM are shown in Figure 4. In order to make the faint fracture tip-diffracted waves visible, the gain was chosen such that amplitudes were clipped at 1% of the maximum value. It can be seen that the body wave (P) and the head wave (H) are in good agreement. The tip-diffracted waves (PdP, PdS) are similar but with small differences in amplitudes. The incomparable event is a guided wave (G) propagating along the fracture, which is present in

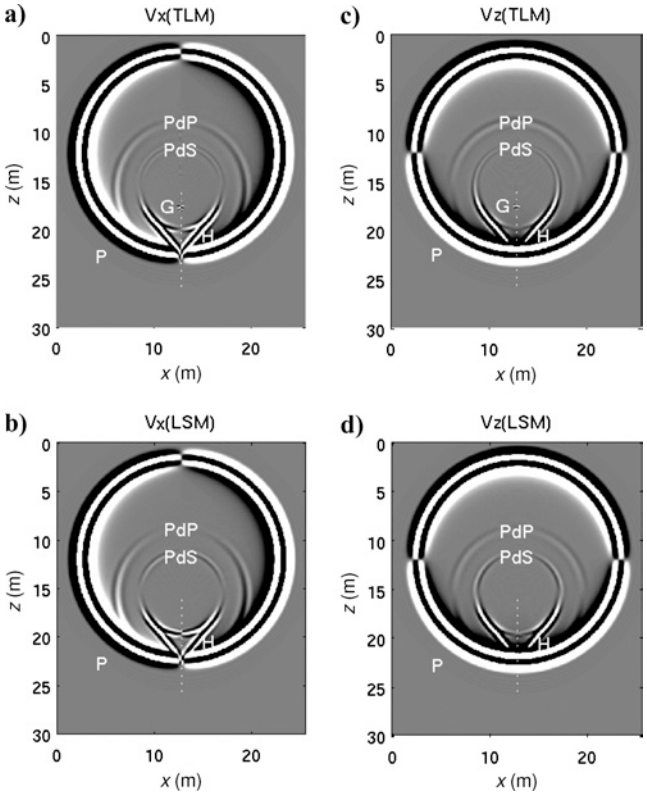

Figure 4. Snapshots of the horizontal and vertical particle-velocity components (V_x and V_z) at 2.8 ms: (a) and (c) are the results of the thin-layer model (TLM); (b) and (d) are the results of the linear-slip model (LSM). P, H, and G are direct P-wave, head wave, and fracture guided wave, respectively; PdP and PdS are P-to-P and P-to-S diffracted waves, respectively. The fracture is indicated by the white dashed line.

the snapshots of the TLM but absent in the snapshots of the LSM. This guided wave, with a velocity around 1210 m/s, is the very slow wave predicted by Ferrazzini and Aki (1987). In theory, the TLM supports a family of symmetric and antisymmetric normal modes (Ferrazzini and Aki, 1987); the LSM supports only one symmetric and one antisymmetric mode (Haugen and Schoenberg, 2000; Pyrak-Nolte and Cook, 1987). Because the symmetry of the source-fracture geometry used in this study (Figure 3) generates only symmetric particle motion with respect to the fracture plane, only symmetric modes are considered in the fracture-guided wave analysis presented in Appendix B. As Figure B-1 shows, except for the slow wave (the fundamental symmetric mode) of the TLM, none of the other symmetric modes is expected in our numerical results because the frequency of interest (3 kHz) is far below the cutoff frequencies of those modes (29.1 kHz for the first symmetric normal mode of the TLM and 20.4 kHz for the symmetric mode of the LSM).

Figure 5 shows the seismograms of the horizontal and vertical particle velocity components recorded off the fracture at receivers R_1 and R_2 of the TLM (blue solid line) and the LSM (red dashed line). The fit between the two models is excellent. The corresponding normalized differences between the two models at these two receivers are shown in Figure 6. We can see that they are all less than 5%. These results quantitatively demonstrate the excellent agreement of the two models for the body waves and fracture tip diffracted waves.

The simulations were performed on a 1.4-GHz Athlon computer with 1-GB DDR RAM. The memory requirements of the two models are comparable (8.7 MB for the TLM and 8.1 MB for the LSM). However, the CPU time used by the TLM (74 minutes) is much longer than that of the LSM (14 minutes). This is due to a very small time-step required by the finest spacing used to satisfy the stability condition (equation 3) in the TLM.

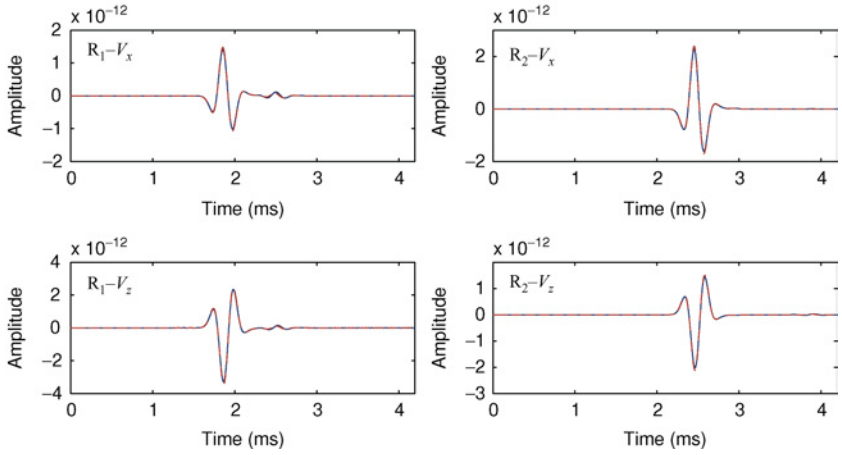

Figure 5. Comparison of seismograms of the horizontal and vertical particle-velocity components (V_x and V_z) of the TLM (blue solid line) and the LSM (red dashed line) at receiver R_1 (left) and R_2 (right) in the model (Figure 3).

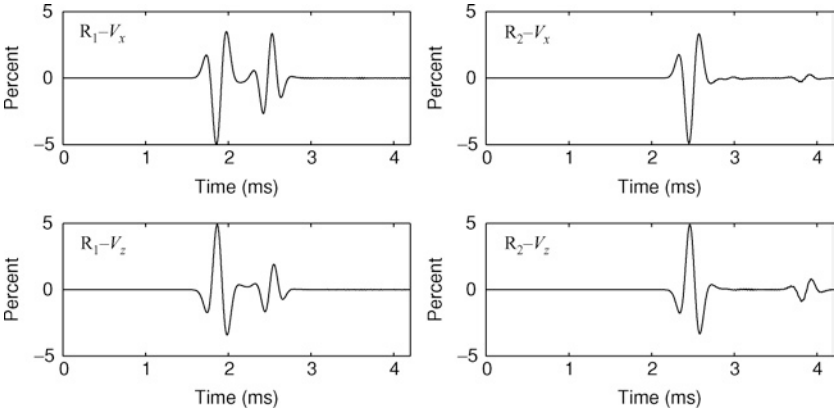

Figure 6. The normalized difference of the horizontal and vertical particle-velocity components (V_x and V_z) between the TLM and the LSM at receiver R_1 and R_2 in the model (Figure 3).

SUMMARY AND CONCLUSIONS

We have compared numerical modeling results for an open water-filled fracture described by the TLM and the LSM. An excellent agreement on body waves and fracture tip diffracted waves has been demonstrated. The primary difference in the observed wavefields of the two models is the presence of a very slow fluid-guided wave in the TLM, which is predicted by the theory and confirmed by the numerical simulations.

In this single-fracture numerical experiment, the computer memory requirements of the two models are comparable. However, the TLM uses five times more CPU time than the LSM. For a set of fractures, the computational cost of the LSM will be significantly less than that of the TLM on both memory and CPU time.

While this comparison study indicates that the TLM is required to model the propagating slow wave in the fluid of an open fracture, this wave would only be observable in a borehole intersecting such a fracture. Thus, for the remote seismic characterization of fractures, the LSM is an efficient and accurate modeling approach.

ACKNOWLEDGMENTS

Discussions with Enru Liu of British Geological Survey during the course of this study provided valuable insight. We thank Michael Schoenberg and two anonymous reviewers for many constructive and helpful comments that significantly improved this manuscript. Financial support for this work was provided by the Assistant Secretary for Fossil Energy, National Petroleum Office of the U.S. Department of Energy under contract No. DE-AC03-76SF00098.

APPENDIX A

FOURTH-ORDER VARIABLE-GRID FINITE-DIFFERENCE OPERATOR

Pitarka (1999) derived a fourth-order staggered-grid FD operator on a variable-grid mesh. We use this operator to approximate the first-order spatial derivatives in equation 1 for efficient modeling of fractures described by the TLM. In this appendix, we briefly review the derivation of this variable-grid FD operator.

Suppose that the field variable g represents one component of particle velocity (v_x, v_z) or stress tensor (τ_{xx}, τ_{zz}, τ_{xz}) in equation 1. The approximation of the first-order derivative of g with respect to x by a fourth-order FD operator on a variable grid spacing dx is given by

$$\frac{\partial g(x,z)}{\partial x} = c_1 g(x+\Delta_1, z) + c_2 g(x-\Delta_2, z) + c_3 g(x+\Delta_3, z) + c_4 g(x-\Delta_4, z), \quad \text{(A-1)}$$

where c_i are four coefficients to be determined. Spatial increments Δ_i can be expressed in terms of the variable grid spacing dx. The increments Δ_i are schematically shown in Figure A-1.

Doing a Fourier transform of equation A-1, we obtain

$$ik = c_1 e^{ik\Delta_1} + c_2 e^{-ik\Delta_2} + c_3 e^{ik\Delta_3} + c_4 e^{-ik\Delta_4}. \quad \text{(A-2)}$$

Using Taylor's expansion up to order $O(\Delta_i^4)$ to approximate the exponentials in equation A-2 and rearranging, we obtain a system of four linear equations:

$$\begin{pmatrix} 1 & 1 & 1 & 1 \\ \Delta_1 & -\Delta_2 & \Delta_3 & -\Delta_4 \\ \Delta_1^2 & \Delta_2^2 & \Delta_3^2 & \Delta_4^2 \\ -\Delta_1^3 & \Delta_2^3 & -\Delta_3^3 & \Delta_4^3 \end{pmatrix} \begin{pmatrix} c_1 \\ c_2 \\ c_3 \\ c_4 \end{pmatrix} = \begin{pmatrix} 0 \\ 1 \\ 0 \\ 0 \end{pmatrix} \quad \text{(A-3)}$$

Solving system A-3, we find the coefficients c_i of the fourth-order variable grid FD operator.

The coefficients c_i are generated prior to the FD calculation, once the variable grid is chosen.

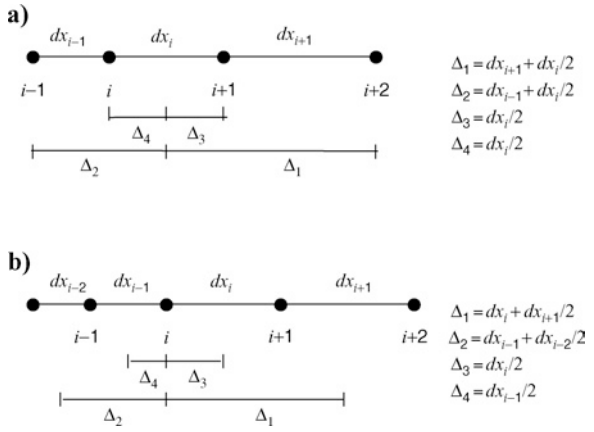

Figure A-1. Grid nodes with variable spacing in the x-direction. Spatial increments Δ_i ($i = 1, 4$) are used to calculate the FD operator centered between (a) the nodes i and $i+1$, and (b) that centered at the node i.

APPENDIX B

FRACTURE-SYMMETRIC WAVE MODES

In this study, the comparison of numerical results between the TLM and the LSM is made on a model with a symmetric source-fracture geometry (Figure 3); therefore, only symmetric wave modes along the fracture will be excited. In theory, the TLM supports a family of symmetric modes and the LSM supports only one symmetric mode. However, we only observe a slow guided wave in the TLM. To explain this, we present the analysis of fracture-symmetric modes in this appendix.

Following Ferrazzini and Aki (1987), the symmetric modes existing along a fracture described by the TLM are given by the following dispersion equations:

$$F = \frac{\rho_f}{q_f}\coth\frac{\omega q_f h}{2} + \frac{\rho_s}{q_p}R(\xi) = 0, \quad \text{for} \quad \xi \geq 1/V_f, \quad \text{(B-1a)}$$

$$\frac{\rho_f}{q_f}\cot\frac{\omega q_f h}{2} - \frac{\rho_s}{q_p}R(\xi) = 0, \quad \text{for} \quad 1/V_s \leq \xi \leq 1/V_f, \quad \text{(B-1b)}$$

where ξ is the phase slowness of the mode; ρ_f and ρ_s are the density of fluid and solid, respectively; h is the fracture aperture; ω is the angular frequency; and R is the Rayleigh slowness relation $R = (2V_s^2\xi^2 - 1)^2 - 4V_s^4\xi^2 q_p q_s$, with the Rayleigh slowness of $R = 0$. The definitions of the qs are $q_f = \sqrt{|\xi^2 - 1/V_f^2|}$, $q_p = \sqrt{|\xi^2 - 1/V_p^2|}$, $q_s = \sqrt{|\xi^2 - 1/V_s^2|}$.

The solution of equation B-1a is the fundamental mode, which exists for all frequencies. The phase velocity of this mode is lower than the fluid velocity for all frequencies and decreases as the frequency decreases. Ferrazzini and Aki call this mode "very slow waves."

Solutions of equation B-1b are a family of normal modes, which exist with ascending series of low cutoff frequencies at $\coth(\omega h q_f/2) = -(\rho_s q_f)/(\rho_f q_p)$ with $\xi = 1/V_s$. The phase velocities of these modes start from the S-wave velocity of the solid at the cutoff frequencies and approach the fluid velocity at high frequencies.

Theoretically, the linear-slip interface (the LSM) has only one symmetric mode, which has the dispersion relation (Haugen and Schoenberg, 2000; Pyrak-Nolte and Cook, 1987)

$$1 - \frac{\omega Z_N}{2}\frac{\rho_s}{q_p}R(\xi) = 0, \quad \text{(B-2)}$$

where Z_N is the normal fracture compliance.

This symmetric interface wave, like the first normal mode in the TLM, has a low frequency cutoff, which is at $\omega = 2\sqrt{1/V_s^2 - 1/V_p^2}/(\rho_s Z_N)$, corresponding to a phase velocity of V_s. But unlike the first normal mode in the TLM, the phase velocity of this symmetric mode approaches Rayleigh wave velocity at high frequencies.

Figure B-1 shows the dispersion curves of the slow wave (the fundamental symmetric mode) and the first symmetric normal mode in the TLM, and the symmetric mode in the LSM with the material parameters of the fracture model in this paper (Figure 3). We can see that the slow wave in the TLM exists for all frequencies, whereas the first normal mode of the TLM and the symmetric mode of the LSM have low cutoff frequencies of 29.1 kHz and 20.4 kHz, respectively. For

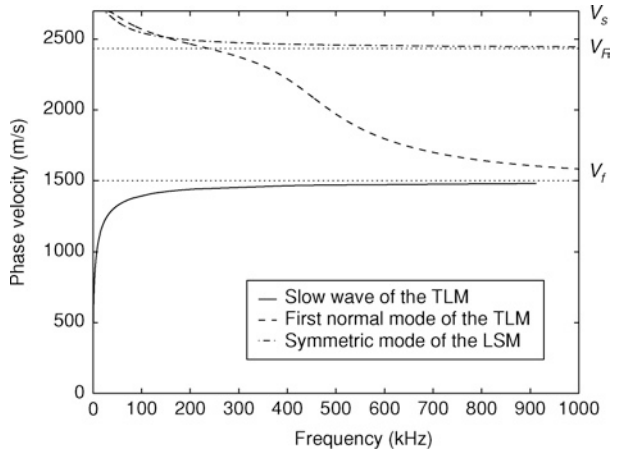

Figure B-1. Phase velocity as a function of frequency for the slow wave (the fundamental symmetric mode), the first symmetric normal mode of the TLM, and the symmetric mode of the LSM. The material properties used are those for the fracture modeling in the text. V_R is the Rayleigh wave velocity.

this model, a source pulse with central frequency of 3 kHz (which is far below the cutoffs) only excites the slow wave in the TLM. The numerical simulations in the paper confirm this theoretical prediction.

The slow wave observed in the snapshots of the TLM is traveling with a velocity around 1210 m/s. From equation B-1a, we obtain a formula to theoretically predict the slow-wave group velocity:

$$v_g = -\frac{\partial_k F}{\partial_\omega F} = \frac{1}{\xi\left(1 - \dfrac{\omega\partial_\omega F}{\xi\partial_\xi F}\right)}. \qquad \text{(B-3)}$$

At 3-kHz frequency, the slow-wave phase velocity is 810 m/s (from Figure B-1); its group velocity calculated from equation B-3 is 1213 m/s, which is very close to that estimated from the numerical results. This further verifies the observed slow wave in the TLM and the used variable-grid FD modeling code.

REFERENCES

Coates, R. T., and M. Schoenberg, 1995, Finite-difference modeling of faults and fractures: Geophysics, **60**, 1514–1526.

Falk, J., E. Tessmer, and D. G. Gajewski, 1996, Tube wave modeling by the finite-difference method with varying grid spacing: Pure and Applied Geophysics, **148**, 77–92.

Ferrazzini, V., and K. Aki, 1987, Slow waves trapped in a fluid-filled infinite crack: Implication for volcanic tremor: Journal of Geophysical Research, **92**, 9215–9223.

Groenenboom, J., and J. Fokkema, 1998, Guided waves along hydraulic fractures: 68th Annual International Meeting, SEG, Expanded Abstracts, 1632–1635.

Groenenboom, J., and J. Falk, 2000, Scattering by hydraulic fractures: Finite-difference modeling and laboratory data: Geophysics, **65**, 612–622.

Haugen, G. U., and M. Schoenberg, 2000, The echo of a fault or fracture: Geophysics, **65**, 176–189.

Jastram, C., and A. Behle, 1991, Elastic modeling by finite-difference and the rapid expansion method: 61st Annual International Meeting, SEG, Expanded Abstracts, 1573–1576.

Levander, A. R., 1988, Fourth-order finite-difference P-SV seismograms: Geophysics, **53**, 1425–1436.

Moczo, P., 1989, Finite-difference technique for SH-wave in 2-D media using irregular grids — Application to the seismic response problem: Geophysics Journal International, **99**, 321–329.

Nihei, K. T., L. Nakagawa, and L. R. Myer, 2001, Fracture imaging with converted elastic waves, *in* D. Elsworth, J. P. Tinucci, and K. A. Heasley, eds., Rock mechanics in the national interest: A. A. Balkema, 1305–1311.

Pitarka, A., 1999, 3D elastic finite-difference modeling of seismic motion using staggered grids with nonuniform spacing: Bulletin of the Seismic Society of America, **89**, 54–68.

Pyrak-Nolte, L. J., 1988, Seismic visibility of fractures: Ph.D. dissertation, University of California at Berkeley.

Pyrak-Nolte, L. J., and N. G. W. Cook, 1987, Elastic interface waves along a fracture: Geophysical Research Letters, **14**, 1107–1110.

Schoenberg, M., 1980, Elastic wave behavior across linear slip interfaces: Journal of the Acoustical Society of America, **68**, 1516–1521.